Flexible Transparent Conductors



# Stretchable Transparent Conductive Films from Long Carbon Nanotube Metals

Peng Wang, Zhiwei Peng, Muxiao Li, and YuHuang Wang\*

Flexible transparent conductors are an enabling component for large-area flexible displays, wearable electronics, and implantable medical sensors that can wrap around and move with the body. However, conventional conductive materials decay quickly under tensile strain, posing a significant hurdle for functional flexible devices. Here, we show that high electrical conductivity, mechanical stretchability, and optical transparency can be simultaneously attained by compositing long metallic double-walled carbon nanotubes with a polydimethylsiloxane substrate. When stretched to 100% tensile strain, thin films incorporating these long nanotubes (≈3.2 µm on average) achieve a record high conductivity of 3316 S cm<sup>-1</sup> at 100% tensile strain and 85% optical transmittance, which is 194 times higher than that of short nanotube controls (≈0.8 µm on average). Moreover, the high conductivity can withstand more than 1000 repeated stretch-release cycles (switching between 100% and 0% strain) with a retention approaching 96%, whereas the short nanotube controls exhibit only 10%. Mechanistic studies reveal that long tubes can bridge the microscale gaps generated during stretching, thereby maintaining high electrical conductivity. When mounted on human joints, this elastic transparent conductor can accommodate large motions to provide stable, high current output. These results point to transparent conductors capable of attaining high electrical conductivity and optical transmittance under mechanical strain to allow large shape changes that may take place in the operation and use of flexible electronics.

Stretchable transparent conductive films (STCFs) can accommodate various configurations on arbitrary surface geometries, leading to intimate contact with objects of different shapes. Such mechanical flexibility is crucial for overcoming the physical mismatch between soft/elastic biological materials and stiff microelectronics.<sup>[1]</sup> Recent advancements in STCFs have initiated a number of exciting applications, such as epi-

P. Wang, Dr. Z. Peng, M. Li, Prof. Y. Wang Department of Chemistry and Biochemistry University of Maryland College Park, MD 20742, USA E-mail: yhw@umd.edu Prof. Y. Wang Maryland NanoCenter University of Maryland College Park, MD 20742, USA

The ORCID identification number(s) for the author(s) of this article can be found under https://doi.org/10.1002/smll.201802625.

DOI: 10.1002/smll.201802625

dermal body sensors,<sup>[2]</sup> implantable retinal prostheses,<sup>[3,4]</sup> and electrophysiology/ neuro-imaging devices.<sup>[5]</sup> Benefitting from higher electrical conductivity, optical transparency, and mechanical stretchability, STCFs can also help build revolutionary applications, like bionic contact lenses, which could potentially superimpose data and information with real vision, thus creating an enhanced reality that could fundamentally change the way humans perceive and interact with the world.<sup>[6–8]</sup>

The major hurdle for further advancement of STCFs, however, has been finding materials that can simultaneously achieve high conductivity (>1000 S cm<sup>-1</sup>) and transparency (>85%) under large tensile strain (>100%). One of the most common approaches to fabricating STCFs is by compositing functional electronic materials with soft substrates.<sup>[1,9]</sup> Currently, conductive polymers, metallic nanostructures, and low-dimensional carbon-based nanomaterials have been successfully proposed as "rigid conductors" for the fabrication of STCFs in combination with elastic polvmers.<sup>[1]</sup> Conductive polymers are inherently flexible and simple to prepare and process, but their intrinsic conductivity is usually low (<550 S cm<sup>-1</sup> at zero tensile

strain). [10,11] Instability caused by environmental factors (e.g., humidity, UV light, and elevated temperature) remains another concern. Micro-sized metals with various structures (e.g., thin films, grids, and nanowires) show excellent electrical performance, but such structures easily delaminate from elastomer substrates at high tensile strain, resulting in quick conductivity decay. [12–15] The hazy appearance of these materials due to their relatively large diameter ( $\approx$ 50 nm) also deteriorates the overall optical transparency. [16] 2D carbon materials, such as graphene, feature superior conductivity and transparency (>5000 S cm<sup>-1</sup> at 85% transmittance) when tensile strain is absent, but readily crack into pieces at less than 5% strain since their carbon–carbon bonding network cannot provide an energy dissipation mechanism to the externally applied force. [17–19]

1D carbon nanotubes (CNTs) are among the most promising candidates for high-performance STCFs. When fabricated into films, CNTs readily assemble into percolating networks that remain intact even at high tensile strain due to the high mechanical strength of these materials (Young's modulus on the order of 1 TPa, as compared with 0.2 TPa for steel). [20]





Additionally, the collective van der Waals interactions between entangled nanotubes ( $\approx$ 0.5 eV nm<sup>-1</sup> for 1.4 nm diameter nanotubes) are much stronger than those from micron-sized 1D metal nanowires, [21] allowing reconfiguration within the CNT network in response to the mechanical strain to avert delamination. [1] Also, CNT films feature high transparency and neutral color, [16] since the small diameter of CNTs can significantly reduce the degree of light scattering and haze effect compared with other 1D metal nanowires. Lastly, recent breakthroughs in mass production (up to 10 tons per year) of high-quality CNTs (OCSiAl's Tuball tubes feature a G/D ratio > 100) had decreased the cost down to \$1 per gram, [22] making CNTs even more competitive than precious metal nanowires or graphene, which is still limited to laboratory-scale production.

Despite the superior flexibility and transparency of CNT-based STCFs, however, a large obstacle is the overall low conductivity of the CNT thin films. While individual CNTs can be extremely conductive, the highest electrical conductivity of macroscale networks formed from raw CNT materials is usually less than 4% of the inherent conductivity of an individual tube. [16] This low conductivity is due to the large junction resistance ( $R_j$ ) between different CNTs. Moreover, raw CNTs are typically synthesized as a polydisperse material that contains both semiconductors and metals, further hampering the use of CNTs as conductive materials.

To alleviate the impact of tube-tube junctions and electron scattering sites on the film conductivity, two strategies can be employed: 1) lowering the average junction resistance and 2) decreasing the number of junctions. In general, junction resistances are much smaller between metallic tubes than their heterogeneous counterparts, which has motivated the development of advanced purification techniques, such as density gradient ultracentrifugation (DGU)[23] and aqueous two-phase extraction, [24] to enrich samples with metallic nanotubes. Additionally, the longer the CNTs, the fewer junctions that are encountered by electrons traversing the fabricated thin films. While methods of growing CNTs with increased lengths have been reported, [25,26] current large-scale fabrication of CNT-based STCFs (such as roll-to-roll processing) typically requires an initial step of dispersing the CNTs into aqueous solution (wet method) using ultrasonication to overcome the strong van der Waals interactions within the CNT bundles. The sonication process, however, inevitably introduces defects and cuts the CNTs into shorter fragments, which is a major issue for further improving the overall conductivities of CNT-based STCFs. To this end, long and metallic CNTs are desirable for high performance devices.

In this work, by compositing full-length metallic outer-walled double-walled carbon nanotubes (m-DWCNTs) as electrical conductors on a polydimethylsiloxane (PDMS) substrate, we successfully fabricated CNT-based STCFs and achieved high electrical conductivity (>1000 S cm<sup>-1</sup>) and high optical transmittance (>85%) at over 200% tensile strain simultaneously. DWCNTs were chosen in this work because previous studies have shown that they are the best type of CNT for high electrical conductivity applications. This is because as the wall numbers increase, individual tubes become more electrically conductive due to the electronic coupling effects between walls, however, the packing density (i.e., number of CNTs

per unit area) in the thin film also decreases. Therefore, the electrical conductivity peaks when the average wall number is approximately two. [28,29] m-DWCNTs were prepared using the simple vet scalable nondestructive superacid-surfactant exchange (S2E) method to first disperse long, raw nanotubes into aqueous solution, followed by subsequent DGU purification to enrich the metallic nanotubes.[30,31] Since no sonication is necessary in this CNT-dispersion and enrichment process, the sorted m-DWCNTs feature an average length of ≈3.2 µm, which is substantially longer than the sonication control (≈0.8 µm on average). Benefiting from this nondestructive process, the fabricated STCFs showed excellent conductor performance. When stretched to 100% tensile strain, 3.2 µm long m-DWCNT STCFs exhibited a record high conductivity of up to 3316 S cm<sup>-1</sup> at 100% tensile strain and superior 85% optical transmittance, which is 194 times higher than that of 0.8 µm short nanotube controls. Moreover, extraordinary electrical stability under prolonged cycles of stretching and release was also observed. After 1000 stretch-release cycles (between 100% and 0% tensile strain), the conductivity of the long m-DWCNT STCFs decayed by just 4%. In contrast, STCFs based on short m-DWCNTs experienced a significant decay of over 89% after the same stretching/releasing protocol. Electron microscopy studies revealed that microscale gaps formed in DWCNT films induced by stretching were effectively bridged by the long nanotubes, which kept the electrical pathways intact throughout the thin film.

Lastly, as a proof of concept to demonstrate the device's use as a flexible conductor, we mounted a 3.2  $\mu m$  long m-DWCNT STCF on a subject's finger, and demonstrated how it can provide a stable electrical current path despite the curling movement of the digit. In contrast the 0.8  $\mu m$  short control demonstrated large electrical current change in response to the finger's movement, suggesting the material's use for sensitive motion sensors. We have systematically studied the length-dependent responsive behaviors of CNT-based conductors, and our results reveal the significant impact of the size of nanoscale components on device performance, paving the way for the application of low-dimensional carbon materials in future flexible electronics.

Figure 1a schematically describes the steps for fabricating STCFs from long m-DWCNTs, including the dissolution of fulllength DWCNTs in aqueous solution using our S2E method, the subsequent purification of m-DWCNTs by the DGU technique, and finally integration of the materials on a PDMS substrate. DWCNTs are dissolved in chlorosulfonic acid (a superacid), which is further exchanged to sodium deoxycholate (DOC) as the superacid-DWCNT solution is added drop by drop into a basic aqueous solution containing the surfactant.[30] The end result is a homogeneous aqueous solution of individual DWCNTs stabilized by DOC. Since there is no sonication-induced cutting, the dissolved DWCNTs maintain their full lengths, which cannot be achieved when sonication is used to disperse the materials. After simple solution-based mixing and filtration steps to concentrate the DWCNTs and remove the salt generated from the neutralization step (see the Experimental Section for details), the obtained DWCNT-DOC aqueous solution can be readily used as the parent material for advanced purification by the established DGU method.

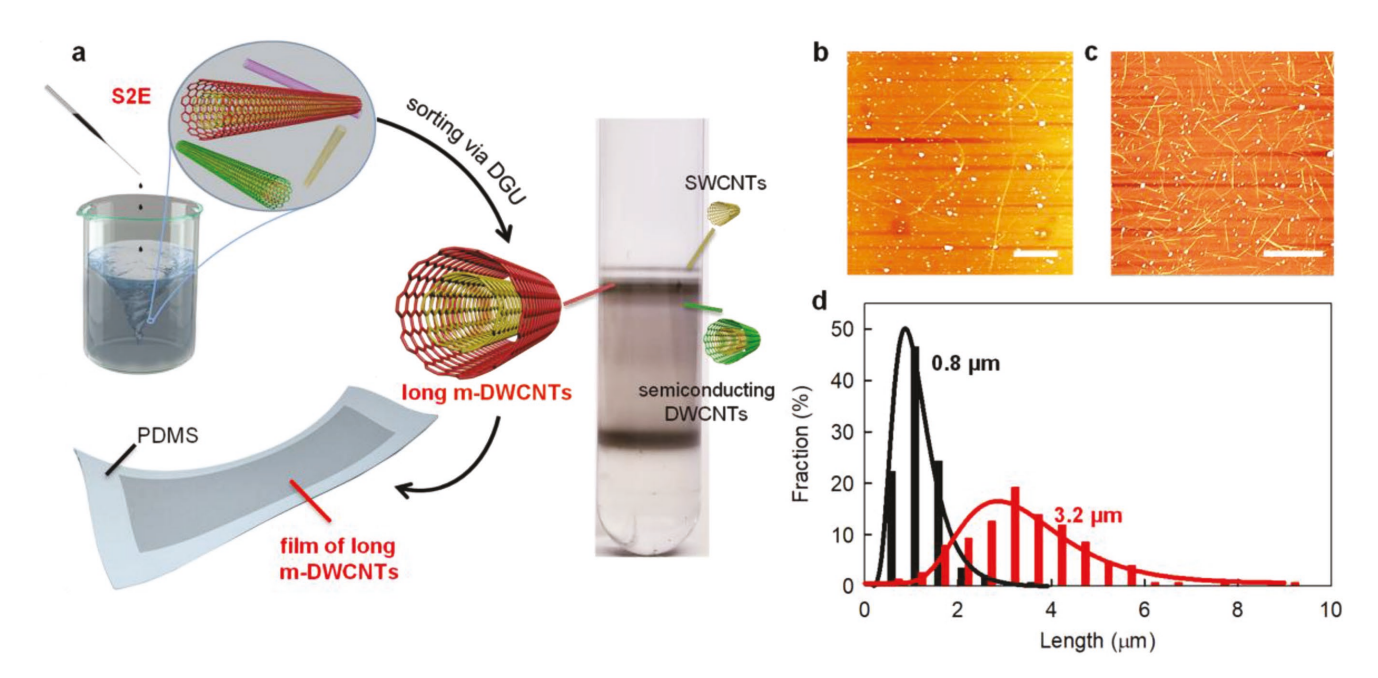


Figure 1. Preparation of long m-DWCNTs. a) Schematic of the fabrication of flexible, transparent, conductive m-DWCNT thin films on PDMS from full-length m-DWCNTs. A photograph of a centrifuge tube following the DGU separation of a S2E-DWCNT solution is shown. Representative AFM topography images of m-DWCNTs prepared by b) S2E and c) sonication. Scale bars: 2 μm. d) Length distribution of long m-DWCNTs (red) and the short sonication control (black).

DGU purification relies on the different buoyant densities of various types of CNTs wrapped by surfactant molecules.<sup>[23,32]</sup> Under a strong centrifugal force, the CNTs will reside in different layers of gradient media that match their buoyant densities. We adopted this DGU method and further modified it to differentiate the electronic type of our S2E DWCNTs by using a co-surfactant system, eventually realizing the separation of m-DWCNTs from single-walled CNTs (SWCNTs) and semiconducting outer-walled DWCNTs (see the Experimental Section for details and Figure S1, Supporting Information). Finally, we filtered the sorted m-DWCNTs to fabricate thin films, which were then transferred onto flexible UV-ozone-treated PDMS substrates to test the samples' electrical properties under various stretching conditions. As controls, DWCNTs were dispersed by a conventional sonication method and sorted by the same DGU procedure to produce short m-DWCNTs, which were fabricated into STCFs for comparison.

We first confirmed the enrichment of m-DWCNTs after S2E dispersion and DGU purification by optical absorption and Raman scattering measurements. Figure 1a shows an ultracentrifuge tube after DGU sorting of the S2E-DWCNTs, which features distinct layers that indicate the enrichment of SWCNTs, m-DWCNTs, and semiconducting DWCNTs from top to bottom, respectively. UV–vis–NIR spectra from each extracted fraction (Figure S1b, Supporting Information) unambiguously demonstrate such assignments: the top fraction showed distinct peaks from 900 to 1350 nm, representing the  $\rm E_{11}$  optical transition of SWCNTs; the middle fraction showed broad absorption between 700 and 900 nm, representing the  $\rm M_{11}$  optical transition of m-DWCNTs; and the bottom fraction exhibited absorption between 900 and 1300 nm, representing the  $\rm S_{22}$  optical transition of semiconducting DWCNTs. [32] Resonant Raman

spectra (Figure S1c,d, Supporting Information) along with transmission electron microscopy (TEM) images (Figure S2, Supporting Information) further demonstrated the separation of SWCNTs, m-DWCNTs, and semiconducting DWCNTs after DGU. Because of the aqueous solution-based nature of the S2E dispersion process, other aqueous separation methods that are less expensive with higher loading, such as aqueous two-phase extraction<sup>[33]</sup> and gel chromatography,<sup>[34]</sup> may also be employed to obtain purified long m-DWCNTs as the starting material for the following experiments.

Atomic force microscopy (AFM) was then used to characterize the length distribution of the sorted m-DWCNTs. Figure 1b,c shows the representative AFM images of the m-DWCNTs from S2E and m-DWCNTs from sonication as the control, respectively. While the m-DWCNTs from sonication featured an average length of 0.8 µm, in substantial contrast the S2E m-DWCNTs reached an average length of 3.2 µm, which is four times longer (Figure 1d). Interestingly, we noticed that the S2E-DWCNTs after DGU featured a slightly larger average length (3.2 µm vs 2.9 µm) (Figure S3, Supporting Information). This increase in the length distribution may be caused by the removal of shorter SWCNTs from the sample during DGU. Due to the fewer wall numbers, SWCNTs tend to grow shorter than the mechanically stiffer DWCNTs during synthesis.[35] Thus, the successive S2E-DGU process proves to be an efficient way of preparing enriched m-DWCNT solutions with maintained nanotube length, which will benefit subsequent device fabrication and performance.

The long purified  $3.2~\mu m$  m-DWCNTs were then used to fabricate thin films of various thicknesses by the filtration method and subsequently transferred onto flexible PDMS substrates for STCF fabrication (see the Experiment Section for details). The sheet resistances of the as-fabricated m-DWCNTs with

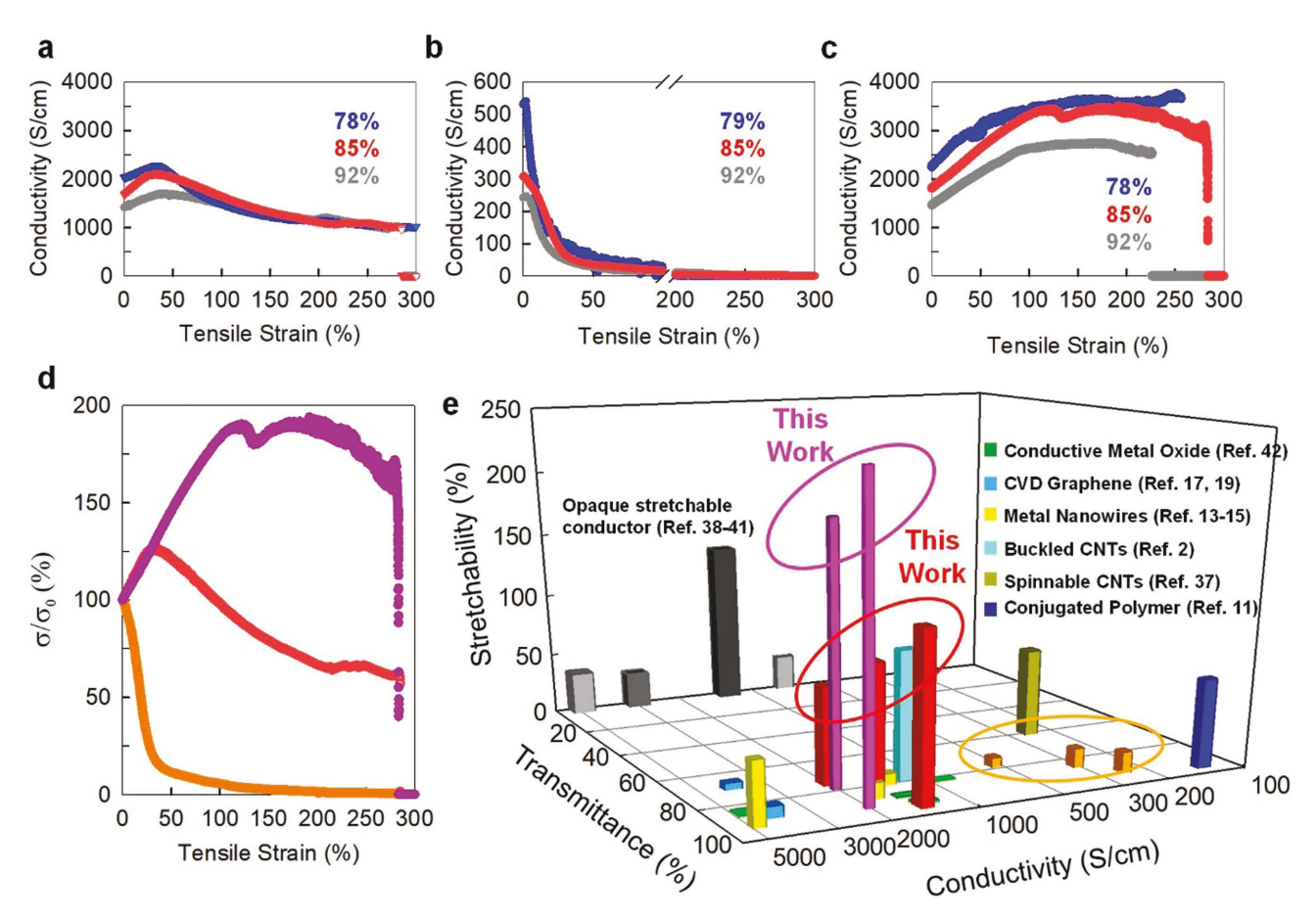


Figure 2. Electrical conductivity versus tensile strain profiles of STCFs fabricated from a) 3.2 μm long m-DWCNTs, b) 0.8 μm short m-DWCNTs, and c) 3.2 μm long m-DWCNTs on prestretched PDMS substrates at various transmittances. The percentages in a–c) indicate the transmittance of different films. d) Normalized conductivity–tensile strain curves of STCFs made from long m-DWCNTs (red), short m-DWCNTs (orange), and prestretched long m-DWCNTs (purple) at 85% transmittance. e) Comprehensive comparison of conductivity, transmittance, and stretchability of STCFs made from long m-DWCNTs (red), short m-DWCNTs (orange), and prestretched long m-DWCNTs (purple) with other reported values.

different optical transmittances were measured using a fourpoint-probe method (Figure S4, Supporting Information) and compared with other publications. Clearly, our films are among the best values reported.[16,32,35,36] The electrical conductivity of the fabricated STCFs were then in situ monitored under tensile stress. Figure 2a,b shows the conductivity as a function of tensile strain for STCFs fabricated from 3.2 µm long m-DWCNTs and 0.8 µm, short m-DWCNTs, respectively, at different transmittances (i.e., film thicknesses). Despite the distinct initial conductivities, all the long m-DWCNTs STCFs of different transparency showed extremely stable and high conductivity under large tensile strain. For example, the conductivity of the STCF at 85% transmittance monotonically increased from an initial conductivity of 1651 S cm<sup>-1</sup> to the maximum value of  $2122~S~cm^{-1}$  when stretched to 32%, possibly due to the straininduced alignment of DWCNTs along the stretching direction, which will be discussed later. Further stretching to 100% strain decreased the conductivity by only 1.8% to 1651 S cm<sup>-1</sup>. Even at 285% tensile strain when the PDMS broke, the conductivity was still maintained as high as 953 S cm<sup>-1</sup>. In contrast, STCFs fabricated from short m-DWCNTs not only showed much lower initial conductivities due to the short length of the tubes and

thus overall high junction resistance, but also manifested pronounced conductivity decay even under minimal tensile strain (<10%), resulting in a conductivity of less than 30 S cm<sup>-1</sup> at 100% tensile strain, which is inadequate for stretchable electronics applications (Figure 2b).

To further increase the mechanical tolerance of STCFs, long m-DWCNTs were deposited onto PDMS substrates that were prestretched to 100% tensile strain (Figure 2c). At 85% transmittance, the conductivity increased from an initial value of 1809 S cm<sup>-1</sup> at 0% strain to 3316 S cm<sup>-1</sup> at 100% tensile strain and 2425 S cm<sup>-1</sup> at a maximum 285% tensile strain. To the best of our knowledge, 2425 S cm<sup>-1</sup> at maximum tensile strain is the record high conductivity for flexible transparent conductive films. We also plotted the normalized conductivity ( $\sigma/\sigma_0$ ) versus tensile strain profile for long m-DWCNT, short m-DWCNT, and prestretched long m-DWCNT STCFs at the same transmittance (85%) in Figure 2d to better show the distinct electromechanical responsive behaviors of these devices. The comparison unambiguously demonstrated the superior mechanical tolerance of longer nanotube-based STCFs (whether prestretched or not) compared with those made from shorter tubes. Notably, in our previous work we demonstrated that the high conductivity

of thin films from S2E-processed CNTs was not the result of doping,[30] which is a commonly used way to increase the conductivity of CNT-based conductive films. Therefore, such STCFs would be an ideal candidate for conductor applications since doped films are not stable and will lose conductivity over time. Figure 2e further provides a comprehensive comparison of the fabricated STCFs from 3.2 µm long m-DWCNTs with previous reported conductors using different conducting materials<sup>[2,11,13–15,17,19,37–42]</sup> to showcase the clear advantage of long m-DWCNTs based STCFs in achieving high performances in all three critical parameters: optical transmittance, electrical conductivity, and mechanical stretchability. To make the comparison more reasonable, we define the stretchability as the tensile strain at which the conductance decreases by 50% (or resistance increases by 200%) of the initial value. Clearly, the conductivity and transmittance of CVD-grown graphene,[17,19] metal nanowires,[13-15] and metal oxide materials,[42] such as indium tin oxide, can be very high (>1000 S cm<sup>-1</sup>), however, most of their stretchabilities are less than 20%. Spinnable CNTs[37] and conjugated polymers[11] can reach a stretchability of more than 70% but their overall conductivities are less than 250 S cm<sup>-1</sup>. Printing conductive ink from Ag flakes or conductive polymers with ionic additives<sup>[38–41]</sup> can generate high conductivity (>1500 S cm<sup>-1</sup>) and modest stretchability (>50%), however, the opaque nature of these inks prevents their use as transparent flexible conductors (films composed of transparent elastomer substrates with printed opaque lines cannot be categorized as "true" STCFs since their inhomogeneous conductive nature prevents their use in applications such as bionic contact lenses).

Long m-DWCNT thin films by simultaneously combining high transmittance (>85%), high conductivity (>1000 S cm<sup>-1</sup>), and high stretchability (>90%) unambiguously outperformed all other reported conductors. Furthermore, the prestretching strategy can further enhance the stretchability of the long m-DWCNTs STCFs to ~200% while maintaining superior transmittance and conductivity. Note that the long m-DWCNTs used here are sorted only by the electronic type of the outerwall through DGU, many of which contain semiconducting inner tubes that can deteriorate the overall conductivity of STCFs. Therefore, further enhancement of conductivity may be achieved by using sorted DWCNTs with metallic inner and outer tubes.[34] Moreover, the length (3.2 µm) of the sorted m-DWCNTs is limited by the average length of the raw material. With further improvement in the synthesis of longer tubes in bulk quantity and length-based separation, our method could eventually lead to even greater performance using ultralong CNT STCFs.

In order to evaluate the durability and reversibility of m-DWCNT STCFs, we used a homemade dynamic mechanical analyzing system to monitor the resistance change of the films over prolonged stretch-release cycles. The resistances of the STCFs at 0% (released state) and 100% (stretched state) tensile strain were measured (**Figure 3a**) and plotted in cycling profiles (Figure 3b−e). The long m-DWCNT STCFs exhibited an extremely stable resistance profile with only 4% increase of the initial value after 1000 stretch-release cycles, corre sponding to only ≈0.004% conductance loss per cycle. In sharp contrast, after 1000 stretch-release cycles, at the released state,

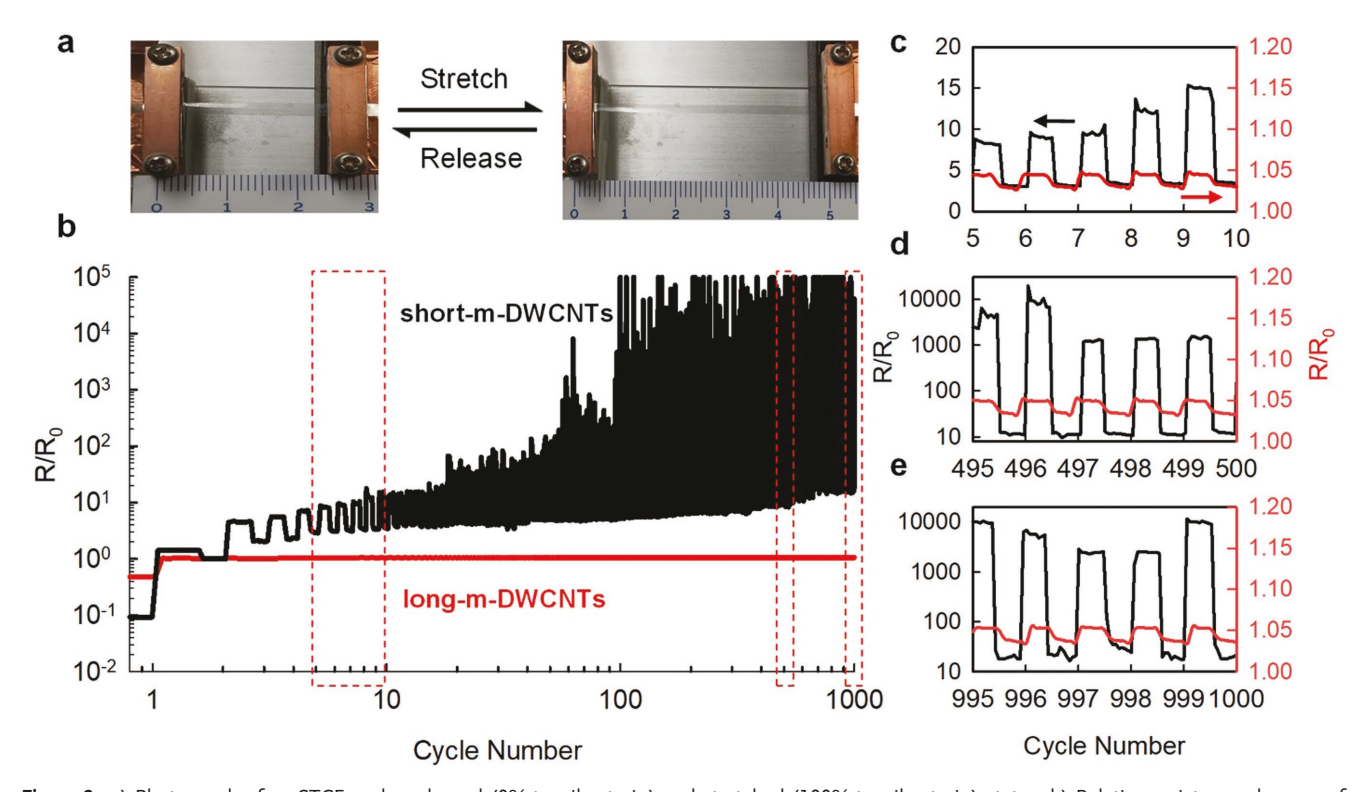


Figure 3. a) Photograph of an STCF under released (0% tensile strain) and stretched (100% tensile strain) states. b) Relative resistance changes of long m-DWCNT (red) and short m-DWCNT (black) STCFs under long term stretching-releasing cycles. c-e) are zoomed-in relative resistance profiles for the stretching-releasing cycles of 5–10, 495–500, and 995–1000, respectively.

the resistance of the short m-DWCNT STCF increased by 19-fold, representing  $\approx 0.095\%$  conductance decay per cycle. Therefore, the durability of STCFs made from long tubes is  $\approx 23.7$  times better than that from short tubes. An abrupt resistance change  $(R/R_0 > 10^5)$  in short m-DWCNT thin films was observed after 100 cycles, which can be explained by the accumulation of "permanent gaps" throughout the film generated after each cycle (see later discussions). We also noticed that the long m-DWCNT STCFs exhibited high conductivity tolerance not only to stretching, but also to other shape deformations, such as rolling, folding, and twisting (Figure S5, Supporting Information).

To fully understand the length-dependent distinct electromechanical responses, scanning electron microscopy (SEM) was used to study the surface morphology of these devices under different strains. Initially, DWCNTs of both short and long lengths assembled into uniform thin films on the top of the PDMS substrate with isotropic orientations (Figure 4a,e). For STCFs comprised of short m-DWCNTs, when applied with 50% strain, nano-sized gaps began to emerge within the thin film (Figure 4b), and further stretching to 100% strain caused the gaps to enlarge to a few hundred nanometers. At this point, the thin film was lacerated into different "patches" (Figure 4c). After the strain was released, the relaxation caused some gaps to recombine together while others stayed permanently open (Figure 4d). On the other hand, thin films made from long m-DWCNTs exhibited a completely different surface morphology change with added stress. At 50% tensile strain, although some nano-sized gaps were also generated, the main phenomenon we observed was the stress-induced

tube-alignment parallel to the stretching direction (Figure 4f). When stretched to 100% strain, gaps of a few hundred nanometers appeared, but in comparison to the short m-DWCNT sample, the long m-DWCNTs were able to successfully bridge these gaps (Figure 4g). After releasing the strain, the long tube bridges formed "wavy structures" across these gaps (Figure 4h). We assume the main reason causing these phenomena is the mismatch of flexibilities between the DWCNT thin films and the PDMS substrate. Briefly, CNT thin films tend to stretch with the UV-ozone-treated PDMS because of strong adhesion force, but their low elasticity compared with PDMS induces breakages across the thin films. Since long tubes can successfully bridge the gaps between different "patches" within the film, active percolating electrical pathways are therefore maintained. In comparison, gaps generated upon stretching the long m-DWCNT STCFs could not be bridged due to the short length of the sonicated tubes, consequently resulting in the fragmentation of electrical pathways and a significant deterioration of conductivity. When the strain is released, some "patches" in the short m-DWCNT STCFs come into contact again to partially resume the electrical connections, but more were permanently disconnected, leading to overall degraded conductivity. As for the long m-DWCNT STCFs, since most electrical pathways were maintained across the gaps during the strain-relaxation cycles, the overall film conductivity changed little if any during mechanical deformation.

Long m-DWCNT STCFs, with their extremely stable conductivities over high tensile strain, should be ideal candidates for wearable electronic applications where stable conductivity

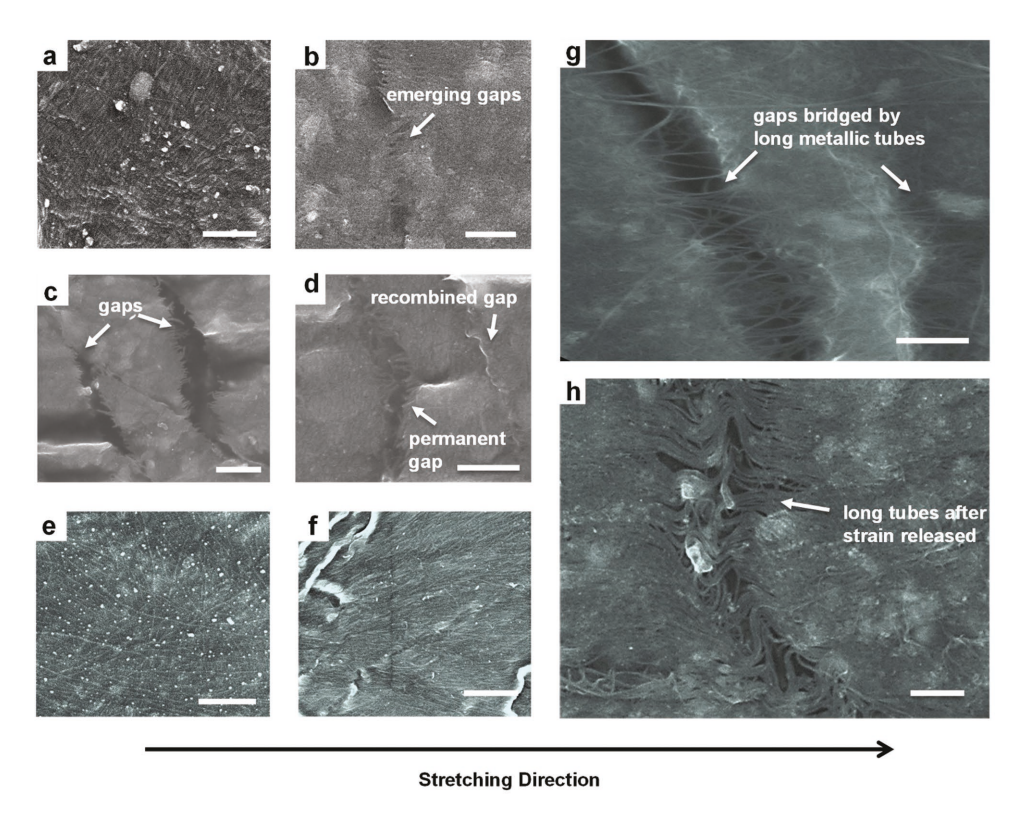


Figure 4. Surface morphology evolution of STCFs made from short m-DWCNTs a-d) and long m-DWCNTs e-h) under different tensile strains, including a,e) 0% tensile strain, b,f) 50% tensile strain, c,g) 100% tensile strain, and d,h) back to 0% tensile strain. All scale bars: 500 nm.

is required in diverse configurations and at different strains. As proof of principle, a long m-DWCNT STCF featuring 85% transmittance was mounted to the joint of an index finger to mimic the motions of the human body in real life and connected to a light-emitting diode (LED) as a real-time indicator of local film conductivity change (Figure 5a). 3 V was applied and the corresponding circuit diagram is shown in Figure S6 in the Supporting Information. Relative changes in conductivity were recorded with multiple cycles of bending/relaxing of the index finger. Figure 5b shows the relative resistance profile of the long m-DWCNT and short m-DWCNT STCFs. The long m-DWCNT STCFs did not show any notable changes in conductivity when the joint was bent, which is consistent with the same brightness of the connected LED light and constant measured current (from 0.151 to 0.150 mA) regardless of the position of the finger (Figure 5c,e and Video S1, Supporting Information). However, for short m-DWCNT STCFs, when the joint was bent, the overall resistance increased by ≈40 times and the measure current dropped from 0.055 mA to 1.376 µA. The connected LED readily responded to this local conductivity change by displaying a weak light when the finger was straight, which was totally extinguished when the finger was bent (Figure 5d,f and Video S2, Supporting Information). While the dramatic conductivity differences are not preferable in flexible conductors, we note the short m-DWCNT STCFs may find application in motion sensors<sup>[43–45]</sup> due to their high sensitivity in response to small shape changes. Figure S7 (see Supporting Information) demonstrates several examples of using the short m-DWCNT STCFs to monitor subtle motions (e.g., swallowing and scowling) of the human body.

In conclusion, we have successfully fabricated STCFs with extraordinarily high and stable conductivity, superior transparency, and stretchability over repeated tensile strain cycles by incorporating long metallic DWCNTs into PDMS. The long nanotubes were obtained by dispersing the materials in water at full-length followed by purification based on their electronic types. The resulting STCFs exhibited a high electrical conductivity of 1809 S cm<sup>-1</sup> at 85% transmittance, which increased to 3316 S cm<sup>-1</sup> at 100% tensile strain, and featured only a 4% decay after 1000 such stretch–release cycles. SEM images reveal that long tubes bridge gaps formed in the thin films during stretching, thus preserving the overall conductivity of the device. On the other hand, short nanotubes showed significantly larger ON/OFF ratios, making them a better candidate as strain sensors.

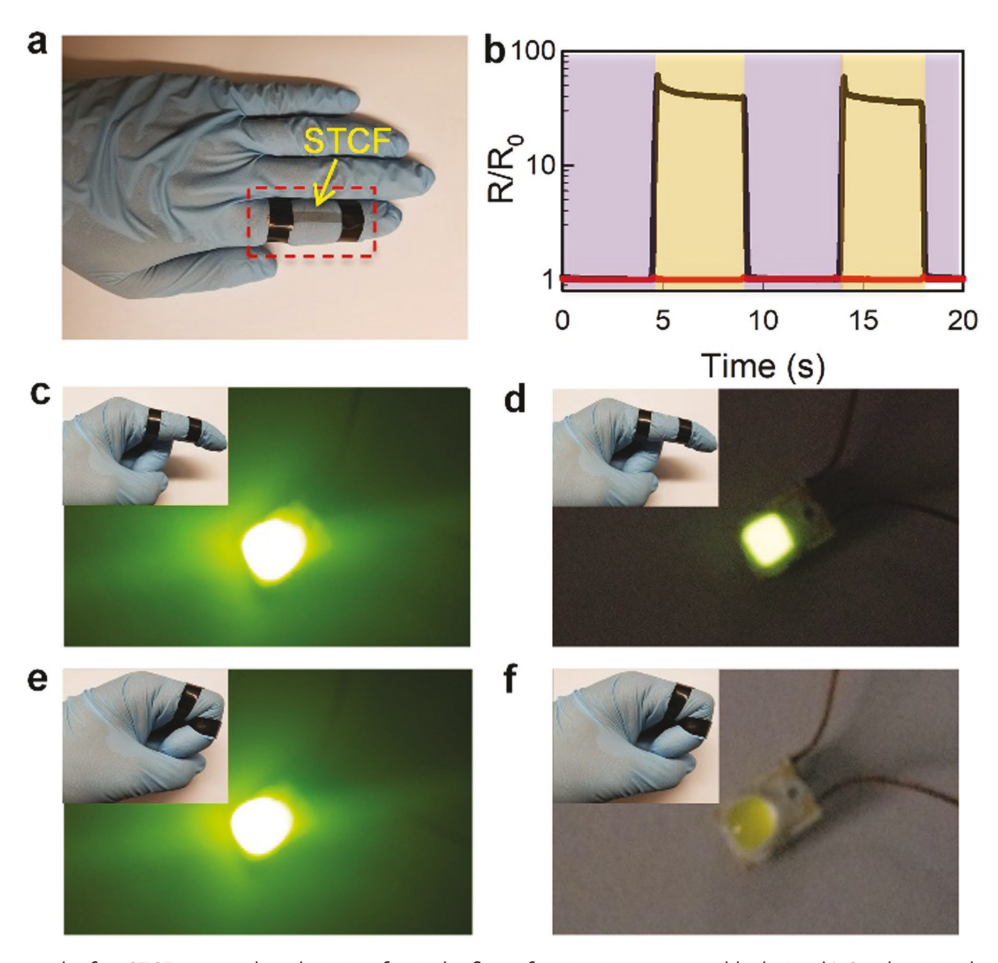


Figure 5. a) A photograph of an STCF mounted on the joint of an index finger functioning as a wearable device. b) Conductivity change of the mounted STCF when the index finger is straightened (purple area) or bent (orange area). Red and black lines are conductivity responses of long m-DWCNT and short m-DWCNT STCFs, respectively. Brightness changes from an LED attached to c,e) long m-DWCNT and d,f) short m-DWCNT STCFs during c,d) straightening and e,f) bending of the index finger.





in air at 300  $^{\circ}$ C for 15 min so that the surfactants and other possible organic solvents could be removed. All AFM images were recorded in tapping mode on a Cypher ES AFM (Asylum Research Corporation) with conical AFM probes backside-coated with gold (Tap300GD-G, with a force constant of 40 N m $^{-1}$ , Ted Pella).

Our results demonstrate the length of CNTs is a critical role governing the collective electromechanical properties of CNT-based conductors allowing transparent conductors to be fabricated from the same CNT materials and tailored for different applications in wearable electronics and human–machine interactive devices.

**Experimental Section** 

Dissolution of Full-length DWCNTs in Aqueous Solution Using the S2E Method: 2 mg of raw DWCNT powder (CheapTubes Inc.) was mixed with 10 mL chlorosulfonic acid (Sigma Aldrich, 99.9%) and stirred using a magnetic stir bar overnight so that the DWCNTs were fully dissolved. The DWCNT-superacid solution was then added drop by drop to 1200 mL of aqueous solution containing 0.05 wt/v% DOC (Sigma Aldrich, ≥97%) and 0.5 M NaOH with vigorous stirring until the final pH value reached ≈8 (Warning: the neutralization process is extremely aggressive and will generate a large amount of acidic smog and heat. All the neutralization experiments should be performed in a fume hood and with protective equipment worn, including acid-resistant gloves, face masks, goggles, and lab coat). The solution was further stirred for 1 h until the pH was stable. Several drops of 0.5  $\,\mathrm{m}$  HCl were then added to decrease the pH of the solution to 5, at which point the DOC molecules were protonated and precipitated out of the solution together with the wrapped DWCNTs (Figure S8, Supporting Information). The precipitates were filtered out using a 47 mm sized PVDF filtration membrane with 0.05 µm pores (Merch Millipore Ltd), then rinsed with 20 mL nanopure water and collected. The resulting dark-gray precipitate was then mixed with 20 mL nanopure water and a few drops of 1 M NaOH aqueous solution, and agitated vigorously using a vortex mixer so that the DOC and DOC-wrapped DWCNTs dissolved. The solution was centrifuged at 23 264 g for 1 h using a benchtop centrifuge (Eppendorf Centrifuge 5810R) to remove undissolved particles. For controls, 1 mg raw DWCNT power was mixed with 10 mL 2% wt/v% DOC solution, tip-sonicated 1.5 h using a tip sonicator (Qsonica S-4000), and centrifuged at 23 264 g for 1 h to remove any large bundles.

Separating m-DWCNTs Using DGU: DGU separation of m-DWCNTs was performed using an Optima XE-90 ultracentrifuge (Beckman Coulter). A linear density gradient was first formed in an open-top polyclear centrifuge tube (Seton) containing homogeneous 0.4% w/v sodium cholate and 0.6% w/v sodium dodecyl sulfate surfactant loading. The density gradient, with water as solvent, consisted of a 1.5 mL underlayer containing 60% w/v iodixanol (Sigma Aldrich), followed by a 5 mL linear gradient with a concentration ranging from 40 to 25% w/v iodixanol generated from a gradient maker (Hoefer SG15). After that, a 1 mL layer of the S2E dispersed DWCNT solution containing 20% w/v iodixanol was added on top of the linear gradient. ≈4 mL of 0% w/v iodixanol solution was finally added to fill the tube. The gradient solutions were then ultracentrifuged for 15 h at a rotational frequency of 40 000 rpm in a SW41 Ti rotor (Beckman Coulter). Following DGU, the sorted materials were extracted using a piston gradient fractionator (Biocomp Instruments) into  $\approx 100~\mu L$  fragments for later characterization.

Spectroscopic and Microscopic Characterization: The UV-vis-NIR absorption spectra of the DWCNT solution before and after DGU purification were measured using a Lambda 1050 (Perkin Elmer) spectrometer equipped with a broadband InGaAs detector. To measure the transmittance of the STCFs, an integrating sphere (Labsphere Model No. 150 MM RSA ASSY) equipped with a broadband InGaAs detector installed in the UV-vis-NIR spectrophotometer was also used. A LabRAM ARAMIS Raman microscope (Horiba Jobin Yvon) was used to measure to the Raman scattering of the DWCNTs before and after DGU sorting. SEM and TEM images were collected with a SU-70 SEM (Hitachi) and a JOEL FEG TEM, respectively.

<code>DWCNT Length Characterization: DWCNTs before and after DGU purification were deposited on (3-aminopropyl) triethoxysilane functionalized  $Si/SiO_2$  substrates. The coated wafers were annealed  $Si/SiO_2$  substrates.</code>

Fabrication and Characterization of STCFs: Dispersed DWCNTs were filtered through a 0.025 µm nitrocellulose membrane (Merch Millipore Ltd) to form light gray thin films of various thicknesses. The PDMS films were fabricated by spin coating the mixture of precursor and Sylgard 184 (Dow Corning) at a ratio of 10:1 on a glass substrate at 500 rpm and cured at 80 °C for 8 h. Prior to transferring the DWCNT thin films onto the PDMS substrate, the PDMS films were treated with 20 min UV-ozone (ProCleaner Plus, Bioforce Nanosciences) with a UV intensity of 19.4 mW cm<sup>-2</sup> to increase the adhesion between the DWCNTs and the PDMS. The DWCNTs along with the filtration membrane were compressed onto the PDMS/glass substrate by applying force and annealed at 90 °C for 1 h. An overnight acetone vapor bath at 105 °C followed by acetone rinsing were used to totally dissolve and remove the filtration membrane. The PDMS/DWCNTs thin film was then peeled off with a razor blade from the glass substrate. Four Ag electrodes were deposited on the as-fabricated STCFs using a Metra Thermal Evaporator in order to facilitate the measurement of the electrical conductivities. A high-speed camera was used to monitor the length and width change of the PDMS/DWCNT composites during the stretching process. AFM was also used to measure the film thickness. A thickness-optical transmittance curve is plotted in Figure S9 in the Supporting Information. For fabricating STCFs for human motion sensor applications, the overall procedure was identical except the PDMS precursor was spin coated on glass substrates at 4000 rpm so the thinner STCFs that were produced could adhere to the human body better. Electrical measurements were carried out using an HMS-5000 semiconductor parameter analyzer and a Biologic SP-200 potentiostat. Mechanical tensile strain tests were performed on a Shimazu Autograph AGS-X tensile tester.

## **Supporting Information**

Supporting Information is available from the Wiley Online Library or from the author.

#### Acknowledgements

P.W. and Z.P. contributed equally to this work. This work was partially supported by AFOSR (FA9550-16-1-0150) and NIH/NIGMS (R01GM114167). AFM images were obtained using a shared system supported by the NSF MRI program (CHE1626288).

#### **Conflict of Interest**

The authors declare no conflict of interest.

### Keywords

carbon nanotubes, nanomaterials processing, responsive materials, transparent conductors, wearable electronics

Received: July 5, 2018 Published online: August 9, 2018

<sup>[1]</sup> J. A. Rogers, T. Someya, Y. Huang, Science 2010, 327, 1603.

<sup>[2]</sup> D. J. Lipomi, M. Vosgueritchian, B. C. Tee, S. L. Hellstrom, J. A. Lee, C. H. Fox, Z. Bao, *Nat. Nanotechnol.* 2011, 6, 788.

www.small-iournal.com

- [3] J. Dowling, Eye 2009, 23, 1999.
- [4] L. Hu, W. Yuan, P. Brochu, G. Gruner, Q. Pei, Appl. Phys. Lett. 2009, 94, 161108.
- [5] D. Kuzum, H. Takano, E. Shim, J. C. Reed, H. Juul, A. G. Richardson, J. De Vries, H. Bink, M. A. Dichter, T. H. Lucas, *Nat. Commun.* 2014, 5, 5259.
- [6] B. A. Parviz, IEEE Spectrum 2009, 46, 36.
- [7] A. R. Lingley, M. Ali, Y. Liao, R. Mirjalili, M. Klonner, M. Sopanen, S. Suihkonen, T. Shen, B. Otis, H. Lipsanen, J. Micromech. Microeng. 2011, 27, 125014.
- [8] M.-S. Lee, K. Lee, S.-Y. Kim, H. Lee, J. Park, K.-H. Choi, H.-K. Kim, D.-G. Kim, D.-Y. Lee, S. Nam, Nano Lett. 2013, 13, 2814.
- [9] D. H. Kim, J. A. Rogers, Adv. Mater. 2008, 20, 4887.
- [10] D. J. Lipomi, J. A. Lee, M. Vosgueritchian, B. C.-K. Tee, J. A. Bolander, Z. Bao, *Chem. Mater.* **2012**, *24*, 373.
- [11] D. J. Lipomi, B. C. K. Tee, M. Vosgueritchian, Z. Bao, Adv. Mater. 2011, 23, 1771.
- [12] Y. Liu, J. Zhang, H. Gao, Y. Wang, Q. Liu, S. Huang, C. F. Guo, Z. Ren, *Nano Lett.* **2017**, *17*, 1090.
- [13] Y. Cheng, S. Wang, R. Wang, J. Sun, L. Gao, J. Mater. Chem. C 2014, 2, 5309.
- [14] W. Hu, R. Wang, Y. Lu, Q. Pei, J. Mater. Chem. C 2014, 2, 1298.
- [15] H. Wu, D. Kong, Z. Ruan, P.-C. Hsu, S. Wang, Z. Yu, T. J. Carney, L. Hu, S. Fan, Y. Cui, Nat. Nanotechnol. 2013, 8, 421.
- [16] D. S. Hecht, L. Hu, G. Irvin, Adv. Mater. 2011, 23, 1482.
- [17] S.-H. Bae, Y. Lee, B. K. Sharma, H.-J. Lee, J.-H. Kim, J.-H. Ahn, Carbon 2013, 51, 236.
- [18] N. Liu, A. Chortos, T. Lei, L. Jin, T. R. Kim, W.-G. Bae, C. Zhu, S. Wang, R. Pfattner, X. Chen, Sci. Adv. 2017, 3, e1700159.
- [19] V. P. Verma, S. Das, I. Lahiri, W. Choi, Appl. Phys. Lett. 2010, 96, 203108.
- [20] N. Yao, V. Lordi, J. Appl. Phys. 1998, 84, 1939.
- [21] L. Girifalco, M. Hodak, R. S. Lee, Phys. Rev. B 2000, 62, 13104.
- [22] https://ocsial.com/en/ (accessed: June 2018).
- [23] M. S. Arnold, A. A. Green, J. F. Hulvat, S. I. Stupp, M. C. Hersam, Nat. Nanotechnol. 2006, 1, 60.
- [24] C. Y. Khripin, J. A. Fagan, M. Zheng, J. Am. Chem. Soc. 2013, 135, 6822
- [25] X. Wang, Q. Li, J. Xie, Z. Jin, J. Wang, Y. Li, K. Jiang, S. Fan, Nano Lett. 2009, 9, 3137.

- [26] S. Huang, M. Woodson, R. Smalley, J. Liu, Nano Lett. 2004, 4, 1025.
- [27] C. Shen, A. H. Brozena, Y. Wang, Nanoscale 2011, 3, 503.
- [28] Z. Li, H. R. Kandel, E. Dervishi, V. Saini, A. S. Biris, A. R. Biris, D. Lupu, Appl. Phys. Lett. 2007, 91, 053115.
- [29] G. Chen, D. N. Futaba, S. Sakurai, M. Yumura, K. Hata, Carbon 2014, 67, 318.
- [30] P. Wang, M. Kim, Z. Peng, C.-F. Sun, J. Mok, A. Lieberman, Y. Wang, ACS Nano 2017, 11, 9231.
- [31] S. Ramesh, L. M. Ericson, V. A. Davis, R. K. Saini, C. Kittrell, M. Pasquali, W. Billups, W. W. Adams, R. H. Hauge, R. E. Smalley, J. Phys. Chem. B 2004, 108, 8794.
- [32] A. A. Green, M. C. Hersam, ACS Nano 2011, 5, 1459.
- [33] J. K. Streit, S. Lam, Y. Piao, A. H. Walker, J. A. Fagan, M. Zheng, Nanoscale 2017, 9, 2531.
- [34] H. Li, G. Gordeev, S. Wasserroth, V. S. K. Chakravadhanula, S. K. C. Neelakandhan, F. Hennrich, A. Jorio, S. Reich, R. Krupke, B. S. Flavel, *Nat. Nanotechnol.* 2017, 12, 1176.
- [35] A. A. Green, M. C. Hersam, Nat. Nanotechnol. 2009, 4, 64.
- [36] F. Mirri, A. W. Ma, T. T. Hsu, N. Behabtu, S. L. Eichmann, C. C. Young, D. E. Tsentalovich, M. Pasquali, ACS Nano 2012, 6, 9737.
- [37] Y. Zhang, C. J. Sheehan, J. Zhai, G. Zou, H. Luo, J. Xiong, Y. Zhu, Q. Jia, Adv. Mater. 2010, 22, 3027.
- [38] K.-Y. Chun, Y. Oh, J. Rho, J.-H. Ahn, Y.-J. Kim, H. R. Choi, S. Baik, Nat. Nanotechnol. 2010, 5, 853.
- [39] N. Matsuhisa, D. Inoue, P. Zalar, H. Jin, Y. Matsuba, A. Itoh, T. Yokota, D. Hashizume, T. Someya, Nat. Mater. 2017, 16, 834.
- [40] N. Matsuhisa, M. Kaltenbrunner, T. Yokota, H. Jinno, K. Kuribara, T. Sekitani, T. Someya, Nat. Commun. 2015, 6, 7461.
- [41] Y. Wang, C. Zhu, R. Pfattner, H. Yan, L. Jin, S. Chen, F. Molina-Lopez, F. Lissel, J. Liu, N. Rabiah, C. Zheng, J. W. Chun, C. Linder, M. Toney, B. Murmann, Z. Bao, Sci. Adv. 2017, 3, e1602076.
- [42] G. Crawford, Flexible Flat Panel Displays, John Wiley & Sons Ltd., Chichester, UK 2005.
- [43] T. Yamada, Y. Hayamizu, Y. Yamamoto, Y. Yomogida, A. Izadi-Najafabadi, D. N. Futaba, K. Hata, Nat. Nanotechnol. 2011, 6. 296.
- [44] L. Cai, L. Song, P. Luan, Q. Zhang, N. Zhang, Q. Gao, D. Zhao, X. Zhang, M. Tu, F. Yang, Sci. Rep. 2013, 3, 3048.
- [45] F. Xu, X. Wang, Y. Zhu, Y. Zhu, Adv. Funct. Mater. 2012, 22, 1279.